JMSR 1(3) (2025)

Journal of Material Science and Radiation

https://journals.balaipublikasi.id/jmsr

Characterization of Photocurable Functionalized-CNT Nanocoating to Mitigate the Naturally Emission of Radon Gas

Aisha Dalila Ab Aziz[1,2], Mohd Hamzah Harun[1*], Izzuddin Mohamad Zaharuddin[1,3], Nor Adnin Ezani Mohd Ezani[1], Norfazlinayati Othman[3], Mahathir Mohamed[1], Mohd Sofian Alias[1], Mohd Faizal Abd Rahman[1], Khairil Nor Kamal Umar[1], Nurul Huda Mudri[1], Khairul Azhar Abdul Halim[1], Mohamad Syahiran Mustafa[4], Lakam Mejus[4], Faizal Azrin Abdul Razalim[5], Rosley Che Ismail[1], Abdul Muiz Mohd Sani[1], Sharilla Mohd Faisal[1], Rida Tajau[1]

[1] Radiation Curing and Synthesis Group, Radiation Processing Technology Division, Malaysian Nuclear Agency, Bangi, 43000, Kajang, Selangor, Malaysia
[2] Department of Physics, Faculty of Science, Universiti Teknologi Malaysia (UTM), 81310 Johor Bahru, Johor, Malaysia
[3] Department of Physics, Faculty of Science, Universiti Putra Malaysia, 43400, Serdang, Selangor, Malaysia
[4] Waste and Environmental Technology Division, Malaysian Nuclear Agency, Bangi, 43000 Kajang, Selangor, Malaysia
[5] Radiation Health and Safety Division, Malaysian Nuclear Agency, Bangi, 43000 Kajang, Selangor, Malaysia

Received: October 24, 2025
Revised: December 11, 2025
Accepted: December 25, 2025
Published: December 31, 2025

Corresponding Author:
Mohd Hamzah Harun
hamzah@nm.gov.my

DOI: 10.56566/jmsr.v1i3.480

Abstract: This study focuses on the synthesis and characterization of an anti-radon photocurable nanocoating formulated using a UV-curable formulation incorporated with functionalized carbon nanotubes (F-CNTs). The coating was prepared using Ebecryl 600 (urethane acrylate oligomer) and TMPTA (monomer), with GPTMS as a coupling agent and various photoinitiator combinations. Different F-CNT loadings ranging from 0.1 to 0.9 wt% were studied to evaluate their effects on coating performance. The samples were cured under UV irradiation for 2–20 passes to investigate the influence of exposure time on polymer crosslinking. Characterization analyses including pendulum hardness, Fourier-transform infrared spectroscopy (FTIR), viscosity, gel content, and radon gas permeability were performed. Results indicated that the incorporation of F-CNTs enhanced the mechanical strength and crosslinking density of the coating. The optimal formulation exhibited a hardness of 150.33 s (BAPO + 8 passes) and a gel content of 97%. Furthermore, radon concentration measurements showed a 28.9% reduction after applying a single coating layer, confirming the coating's potential as an effective barrier for radon gas mitigation.

Keywords: Anti-radon coating; Functionalized carbon nanotubes; Photocurable nanocoating; UV-curable polymer.

Introduction

Radon (^{222}Rn) is a naturally occurring radioactive gas generated from the decay of uranium present in soil, rocks, and construction materials (Ahmad et al., 2017; Veselska et al., 2025). Continuous exposure to radon poses severe health hazards, particularly lung cancer, due to the inhalation of its alpha-emitting progeny (Kashkinbayev et al., 2025). According to the World Health Organization (WHO, 2023), radon is responsible for approximately 14% of lung cancer deaths globally, making it the second leading cause of lung cancer after smoking. In addition, the U.S. Environmental Protection Agency (EPA, 2024) has set the recommended action level for indoor radon concentration at 148 Bq/m³ (4 pCi/L), above which mitigation measures are strongly advised (Cofone et al., 2025; Mphaga et al., 2024; Kellenbenz et al., 2021). These findings highlight the urgent need to develop effective radon mitigation technologies for residential and industrial applications (Kang et al., 2019; Liu et al., 2025).

Meanwhile, radiation-curable coatings, especially those cured under ultraviolet (UV) light, have gained significant interest for sustainable surface protection due to their rapid polymerization, solvent-free formulation, and excellent crosslinking properties (Alias et al., 2025).

How to Cite:
Aziz, A. D. A., Harun, M. H., Zaharuddin, I. M., Ezani, N. A. E. M., Othman, N., Mohamed, M., … Tajau, R. Characterization of Photocurable Functionalized-CNT Nanocoating to Mitigate the Naturally Emission of Radon Gas. *Journal of Material Science and Radiation*, *1*(3), 104–110. https://doi.org/10.56566/jmsr.v1i3.480

The integration of nanomaterials into such systems has shown promising improvements in performance (Crivello and Bulut, 2005). Among various nanomaterials, functionalized carbon nanotubes (F-CNTs) have demonstrated outstanding mechanical strength (Harun et al., 2018), chemical stability (Harun, 2017), and ability to enhance barrier properties by increasing the tortuosity of gas diffusion pathways within polymer matrices (Park and Kim, 2021; Kim et al., 2012).

In this study, an anti-radon photocurable nanocoating was synthesized and evaluated to develop a protective layer capable of reducing radon gas diffusion. The coating formulation consisted of Ebecryl 600 (urethane acrylate oligomer) and trimethylolpropane triacrylate (TMPTA) as the base matrix, GPTMS as a coupling agent, and F-CNTs as nanofillers. Different photoinitiator systems, TPO-L combined with Irgacure 184, BAPO, Irgacure 500, and TPO-L/BAPO blends were utilized to optimize curing efficiency.

Method

The anti-radon photocurable nanocoating was formulated using Ebecryl 600 (Allnex), a urethane acrylate oligomer, and trimethylolpropane triacrylate (TMPTA, Allnex) as the reactive monomer. A silane coupling agent, 3-glycidyloxypropyltrimethoxysilane (GPTMS, Sigma), was incorporated at 1 wt% to enhance interfacial bonding between the polymer matrix and the functionalized carbon nanotubes (F-CNTs). The F-CNTs were introduced as nanofillers with varying loadings from 0.1 to 0.9 wt% to study their effect on the mechanical and barrier properties of the coating. Different photoinitiator systems were prepared to evaluate the effect of curing behavior on coating performance. The photoinitiators used include TPO-L (1.0 g) (BASF) combined with 0.3 g Irgacure 184 (BASF), 1.5 g BAPO (BASF), Irgacure 500 (1.5 g), and a blend of TPO-L (0.8 g) with BAPO (0.7 g). Acetone was used as a solvent and dispersion medium for F-CNTs prior to blending. The formulations were mixed using a mechanical stirrer (Heidolph RZR 2051 Control) operating at 290 rpm for 5 minutes, followed by ultrasonication using a Sonics Vibra-Cell processor at 50% amplitude with a 2-second pulse for 30 minutes to ensure uniform dispersion of nanotubes. The coating formulations were applied onto clean glass substrates using a 50 μm gap applicator rod and a paint brush for even film distribution. Coated samples were cured under UV irradiation using a conveyor-type UV curing machine operating at a constant speed of 10 m/min, with UV exposure varied between 2 and 20 passes. The samples were then stored at room temperature before characterization. Radon permeability was assessed using a portable radon analyzer to evaluate the coating's ability to reduce radon gas diffusion through a concrete culvert. Both coated and uncoated surfaces were tested under identical conditions for 30 minutes to determine changes in radon concentration (Dose, 2022). The measurement setup is shown in Figure 1, where the radon analyzer was connected to a sealed concrete culvert coated with the synthesized formulation. The setup was positioned in an open-air environment to simulate realistic exposure conditions while minimizing background interference.

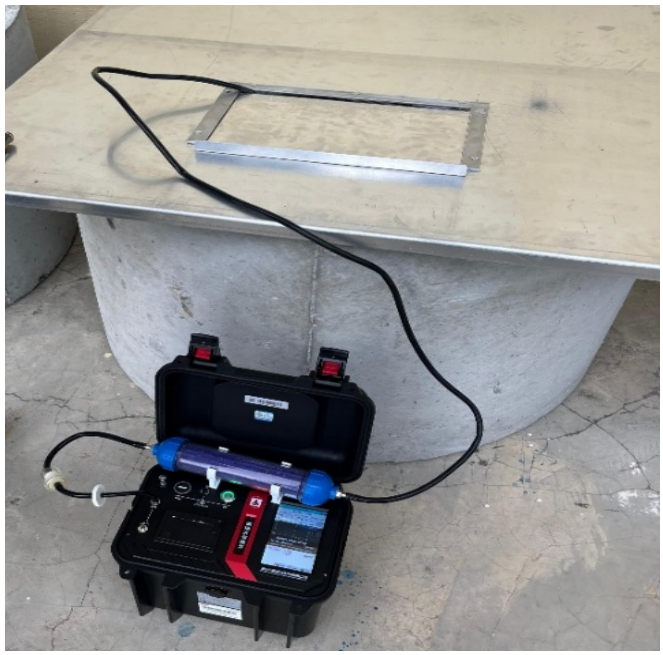

Figure 1. Experimental setup for radon permeability test using a portable radon analyzer on coated and uncoated concrete culvert samples.

Result and Discussion

The performance of the synthesized UV-curable nanocoating was evaluated through pendulum hardness, FTIR spectroscopy, gel content, viscosity, and radon permeability analyses. The results demonstrate the influence of photoinitiator type, UV exposure, and F-CNT loading on the mechanical, chemical, and barrier properties of the developed coatings.

Pendulum Hardness

The pendulum hardness test was conducted to determine the surface rigidity of the cured coatings. As shown in Figure 2, the hardness increased significantly with optimized photoinitiator composition and UV curing passes. The combination of BAPO photoinitiator with 8 UV passes produced the highest hardness value of 150.33 s, indicating superior crosslinking and polymerization efficiency (Alias, 2022). This improvement is attributed to BAPO's deeper UV

absorption and higher initiation efficiency (Cunningham et al., 1994). Beyond the optimal number of passes, a slight decline in hardness was observed, likely due to overexposure and localized heat buildup that may lead to microstructural stress (Bezek and William, 2023). Error bars in Figure 2 represent standard deviations from triplicate measurements, indicating consistent repeatability of results.

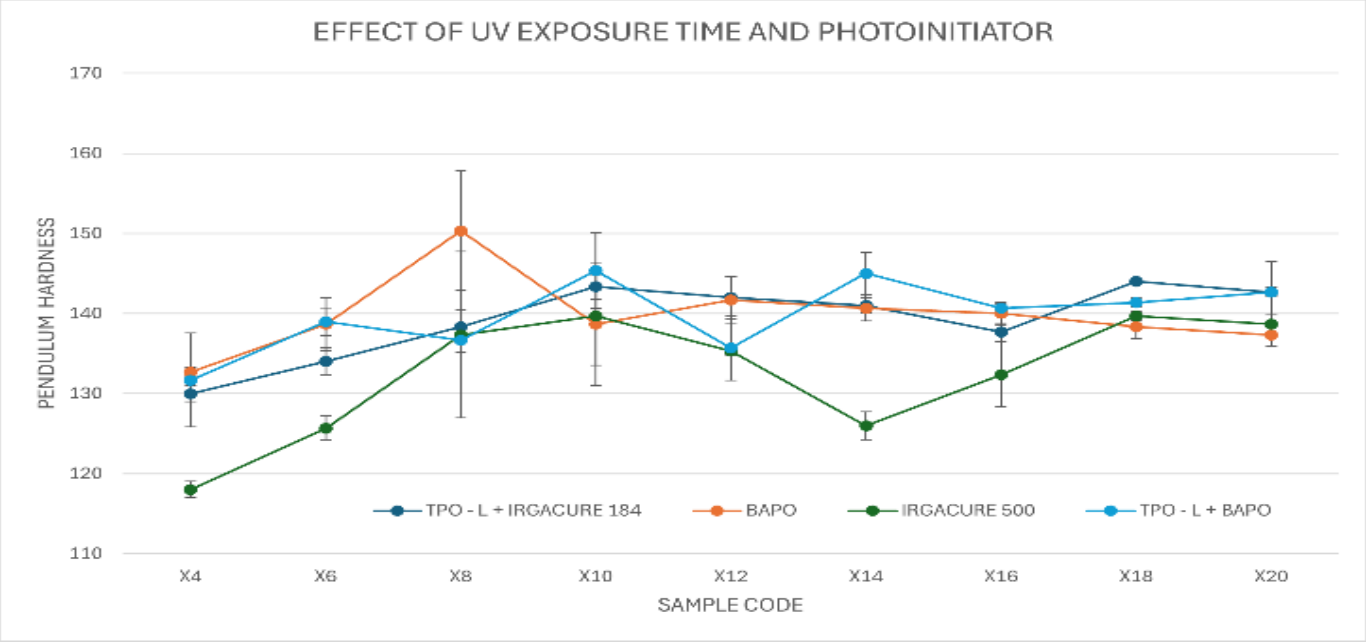

Figure 2. Effect of different photoinitiator systems and UV passes on the pendulum hardness of UV-cured nanocoatings.

Gel Content

The gel content analysis results, presented in Figure 3, reveal that the degree of crosslinking varied with F-CNT loading. The maximum gel content of 97% was recorded at 0.3 wt% F-CNT, signifying a highly crosslinked network with minimal soluble fraction. Lower F-CNT concentrations provided insufficient reinforcement, whereas excessive loading (>0.5 wt%) led to particle agglomeration, limiting UV light penetration and reducing crosslinking efficiency (Diekmann et al., 2021). This correlation confirms that an optimal nanofiller concentration enhances the polymer network's integrity and stability (Rashid, 2024).

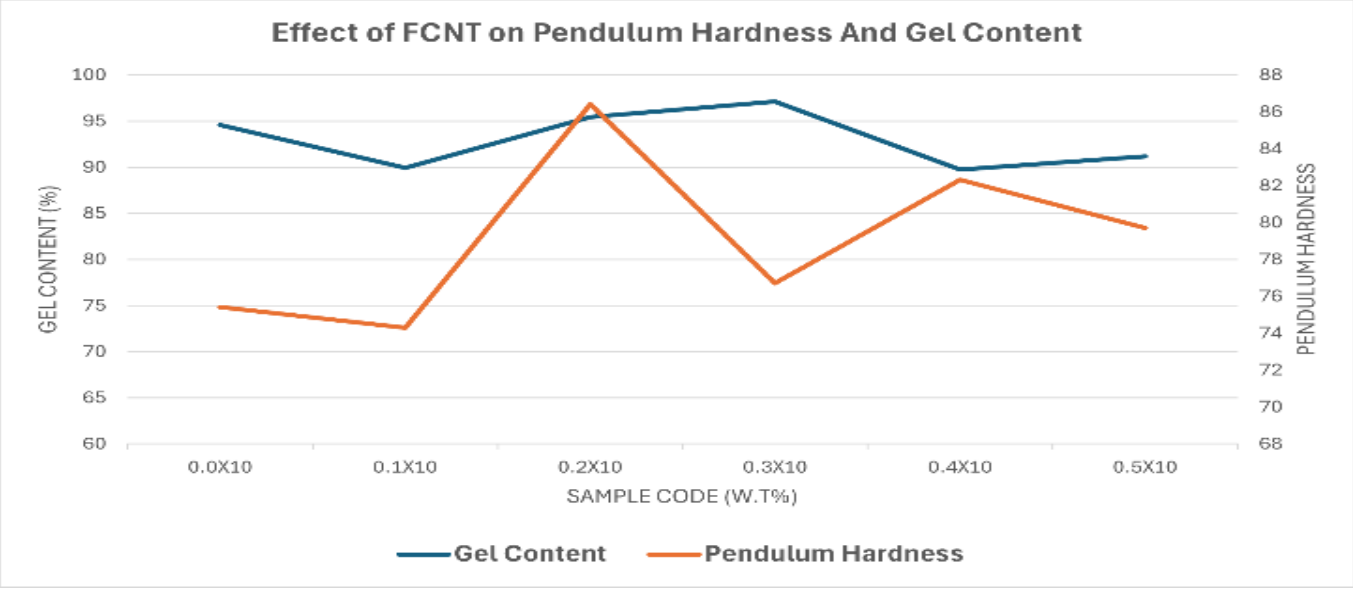

Figure 3. Effect of F-CNT loading on gel content (%) of UV-cured nanocoatings.

FTIR Analysis

The FTIR spectra of uncured and UV-cured samples are presented in Table 1. The disappearance of the characteristic C=C stretching vibration near 1635 cm^{-1} after curing indicates complete conversion of acrylate groups (Alias et al., 2025). The appearance of Si–O–Si

stretching peaks around 1100 cm^{-1} confirms silane crosslinking from GPTMS, which improves interfacial bonding between the F-CNTs and polymer matrix (Jena and Raju, 2008). The intensity of C=O stretching at 1720 cm^{-1} remained stable, suggesting structural integrity of the urethane acrylate backbone after UV curing (Decker, 2002).

Table 1. FTIR spectra of UV-cured nanocoatings showing characteristic peaks before and after curing.

Wavenumber (cm^{-1})	Functional Group	Observation	Correlation to Hardness
3700–3000	O–H / N–H stretching	Decreased with F-CNT due to bonding	Lower peak = stronger interaction
~1720	C=O stretching	Ester/urethane linkage	Sharper peak = stronger structure
~1635	C=C stretching	Unreacted acrylate bonds	Lower intensity = higher curing
~1100	Si–O–Si stretching	GPTMS siloxane network	Sharper peak = better crosslinking
1500-1000	Fingerprint region	CNT–polymer interaction	More details = stronger bonding

Viscosity Analysis

Viscosity measurements were conducted at rotational speeds of 0.3, 0.5, and 1.0 rpm to evaluate the rheological behavior of the coating formulations. The results, as shown in Figure 5, indicate that viscosity increased with higher F-CNT loading, reflecting enhanced intermolecular interactions and network formation within the UV-curable system (Li et al., 2023). At lower loadings (≤0.2 wt%), the coatings maintained uniform flow behavior suitable for application, while excessive F-CNT content (>0.7 wt%) caused a sharp rise in viscosity due to nanotube entanglement and reduced dispersion homogeneity (Khoswan et al., 2024). It was observed that some readings at higher filler concentrations, specifically at 0.4 wt% and 0.7 wt% (1.0 rpm), could not be detected by the viscometer and were recorded as "EEE" in the dataset. This anomaly is attributed to the high viscosity and non-Newtonian behavior of the formulations, which exceeded the instrument's detection range at that rotational speed (Barnes, 2001). The observation supports the strong influence of F-CNT incorporation on thickening and gelation behavior in the coating matrix (Hossain et al., 2025). Overall, the shear-dependent decrease in viscosity with increasing rpm confirms the pseudoplastic (shear-thinning) characteristics typical of UV-curable nanocomposite coatings, where viscosity decreases under shear stress due to the alignment of polymer chains and nanofillers during rotation (Kotsilkova and Tabakova, 2023; Hsissou et al., 2020).

Table 2. Effect of F-CNT loading on viscosity of UV-curable nanocoating at different rotational speeds.

F-CNT Content (wt%)	Viscosity (cP) at 0.3 rpm	Viscosity (cP) at 0.5 rpm	Viscosity (cP) at 1.0 rpm
0.0	4245	3827	3808
0.1	3435	3418	3283
0.2	6059	5939	6003
0.3	5376	5478	4685
0.4	8917	8141	Undetectable
0.5	7701	5734	4474
0.7	13890	10560	Undetectable
0.9	10990	6848	4941

Radon Permeability Test

The radon permeability performance reading shows that the average radon concentration for the uncoated concrete sample was 28.77 Bq/m^3, while the coated surface recorded a significantly lower concentration of 20.46 Bq/m^3 after a 30-minute exposure period. This corresponds to an approximate 28.9% reduction in radon transmission, validating the coating's effectiveness as a diffusion barrier (Ruvira et al., 2022). The reduction is attributed to the dense polymeric film formed after curing, which sealed micro-pores and restricted gas pathways. Furthermore, F-CNT reinforcement increased the tortuosity of radon diffusion, forcing gas molecules to take longer, more complex paths through the material (Kim et al., 2012). Minor variations in readings were observed due to environmental changes such as humidity and temperature (Huang et al., 2024); however, the overall downward trend confirms consistent radon-blocking behavior.

Table 3. Comparison of radon concentration between uncoated and coated concrete samples

Reading	Uncoated Surface		1-Layer Coated Surface	Error
	Radon Concentration	Error	Radon Concentration	
1	20.9	11.68	15.86	10.57
2	20.9	11.76	18.39	10.31
3	44.52	5.94	27.15	3.91
Average	28.77	6.46	20.46	8.26

Conclusion

The synthesis and characterization of the UV-curable anti-radon photocurable nanocoating were successfully carried out using Ebecryl 600, TMPTA, and functionalized carbon nanotubes (F-CNTs) as key formulation components. The combination of optimized photoinitiators and UV exposure parameters produced a uniform, highly crosslinked film with superior surface hardness and structural integrity. Among all systems, the formulation containing BAPO photoinitiator cured at 8 passes demonstrated the highest pendulum hardness (150.33 s), indicating optimal polymerization and mechanical stability. The FTIR analysis confirmed successful chemical bonding and complete acrylate conversion, while gel content measurements revealed a maximum of 97% crosslinking at 0.3 wt% F-CNT loading. Viscosity results showed that increasing F-CNT concentration enhanced intermolecular interactions, though excessive loading caused aggregation and non-uniform flow behavior. The radon permeability test demonstrated a clear improvement in barrier performance, with the coated concrete showing a 28.9% reduction in radon concentration compared to the uncoated surface, confirming its effectiveness as a partial diffusion barrier. In conclusion, the developed photocurable nanocoating exhibits excellent mechanical strength, high curing efficiency, and promising potential for environmental protection and radiation safety applications. The incorporation of F-CNTs not only reinforced the polymer structure but also enhanced the coating's ability to restrict radon gas transmission. For future work, further improvement may be achieved by optimizing nanofiller dispersion techniques, increasing coating layer thickness, or extending UV curing conditions to achieve complete surface sealing. Additionally, long-term stability and multi-layer coating studies are recommended to evaluate durability under various environmental conditions.

Acknowledgments
The authors would like to thank Agensi Nuklear Malaysia (ANM) for providing the facilities and support needed to complete the research work.

Author Contributions
All authors jointly contributed to the writing of this article.

Funding
This research was funded by MOSTI through Strategic Research Fund with a grant number SRF12211190APP.

Conflicts of Interest
The authors declare no conflict of interest.

References

Ahmad, N., Khan, I. U., Rehman, J., & Nasir, T. (2017). An overview of radon concentration in Malaysia. *Journal of Radiation Research And Applied Sciences*, 10(4), 327-330. https://doi.org/10.1016/j.jrras.2017.08.001

Alias, M. S., Othman, N. K., Kamarudin, S. R. M., Harun, M. H., Mohamed, M., Saidin, N. U., Mohamad, S. F. & Samsu, Z. (2022). Influence of graphite particles in UV-curable corrosion protection coating from palm oil based urethane acrylate (POBUA). *Industrial Crops and Products*, 187, 115436. https://doi.org/10.1016/j.indcrop.2022.115436

Alias, M. S., Zulkafli, R., Othman, N. K., Jamil, M. S. M., Kamarudin, S. R. M., Mohamad, S. F., Harun, M. H. & Mohamed, M. (2025). Improving Corrosion Protection of Urethane Acrylate UV Curable Coatings Derived from Palm Oil via Graphene Oxide Particle Incorporation. *Sains Malaysiana,* 54(2), 589-599.

Barnes, H. A. (2001). An examination of the use of rotational viscometers for the quality control of non-Newtonian liquid products in factories. *Applied Rheology,* 11(2), 70-101. https://doi:10.1515/arh-2001-0006

Bezek, L. B., & Williams, C. B. (2023). Process-structure-property effects of ultraviolet curing in multi-material jetting additive manufacturing. Additive Manufacturing, 73, 103640. https://doi.org/10.1016/j.addma.2023.103640

Cofone, L., Sabato, M., Colombo, C., Scalingi, S., Montesi, A., Paglione, L., & Patania, F. (2025). Health Effects and Preventive Strategies for Radon Exposure: A Systematic Review of the Literature. Journal of Respiration, 5(4), 16. https://doi.org/10.3390/jor5040016

Crivello, J. V., & Bulut, U. (2005). Radiation curable coatings and inks containing nanomaterials. *Progress in Organic Coatings, 52*(2), 109–120. https://doi.org/10.1016/j.porgcoat.2004.11.001

Cunningham, A. F., Desobry, V., Dietliker, K., Hüsler, R., & Leppard, D. G. (1994). Recent developments in radical photoinitiator chemistry. *Chimia,* 48(9), 423-423.

Decker, C. (2002). Kinetic study and new applications of UV radiation curing. *Macromolecular Rapid Communications, 23*(18), 1067–1093. https://doi.org/10.1002/marc.200290012

Diekmann, A., Omelan, M. C., & Giese, U. (2021). Influence of carbon nanotube-pretreatment on the properties of polydimethylsiloxane/carbon nanotube-nanocomposites. *Polymers,* 13(9), 1355. https://doi.org/10.3390/polym13091355

Dose, M. (2016). *Reducing Radon Gas Emission in Concrete* (Phd. thesis). KTH Royal Institute of Technology, Stockholm, Sweden.

Harun, M. H., Salleh, N. G. N., Alias, M. S., Mohamed, M., Abdul Rahman, M. F., Hamzah, M. Y. & Othman, N. (2018). Removal of Oxidative Debris from Chemically Functionalized Multi-walled Carbon Nanotube (MWCNT). *International Journal of Nanoelectronics & Materials*, 11(1). https://ijneam.unimap.edu.my/images/PDF/IJNEAM%20No.%201%202018%20JAN/Vol_11_No_1_2018_5_43-48.pdf

Harun, M. H. (2017). Carbon Nanotubes and Radiation Applications in its Synthesis. Chapter 7. *Ionizing Radiation Processing Technology* (pp. 153-169), Malaysian Nuclear Agency.

Hossain, M. M., Chowdhury, H. I., Siddiqui, M. S., Hossain, M. S., & Rabbi, M. S. (2025). Recent Advances in Coated Carbon Nanotube-Reinforced Metal Matrix Composites: Challenges, Techniques, and Performance Enhancement. *Carbon Trends,* 100568, 1-36. https://doi.org/10.1016/j.cartre.2025.100568

Hsissou, R., Bekhta, A., Dagdag, O., El Bachiri, A., Rafik, M., & Elharfi, A. (2020). Rheological properties of composite polymers and hybrid nanocomposites. Heliyon, 6(6) https://doi:10.1016/j.heliyon.2020.e04187

Huang, P., Lv, W., Huang, R., Feng, Y., Luo, Q., Yin, C., & Yang, Y. (2024). Impact of environmental factors on atmospheric radon variations at China Jinping Underground Laboratory. *Scientific Reports,* 14(1), 31402. https://doi:10.1038/s41598-024-82936-0

Jena, K. K., & Raju, K. S. N. (2008). Synthesis and characterization of hyperbranched polyurethane hybrids using tetraethoxysilane (TEOS) as cross-linker. *Industrial & Engineering Chemistry Research*, 47(23), 9214-9224. https://0.1021/ie800884y

Kang, J. K., Seo, S., & Jin, Y. W. (2019). Health effects of radon exposure. *Yonsei Medical Journal,* 60(7), 597-603. https://doi.org/10.3349/ymj.2019.60.7.597

Kashkinbayev, Y., Kazhiyakhmetova, B., Altaeva, N., Bakhtin, M., Tarlykov, P., Saifulina, E., Aumalikova, M., Ibrayeva, D., & Bolatov, A. (2025). Radon Exposure and Cancer Risk: Assessing Genetic and Protein Markers in Affected Populations. *Biology,* 14(5), 506. https://doi.org/10.3390/biology14050506

Kellenbenz, K. R., & Shakya, K. M. (2021). Spatial and temporal variations in indoor radon concentrations in Pennsylvania, USA from 1988 to 2018. *Journal of Environmental Radioactivity,* 233, 106594. https://doi.org/10.1016/j.jenvrad.2021.106594

Khoswan, I., Abusafa, A., & Odeh, S. (2024). The effect of carbon nanotubes on the viscosity and surface tension of heat transfer fluids—A review paper. *Energies,* 17(22), 5584. https://doi.org/10.3390/en17225584

Kim, S. H., Lee, K. H., Kim, D. H., Kim, M. J., Jung, K. S., & Cho, S. Y. (2012). Radon mitigation efficiency using nano-size carbon colloid. *Technical Proceedings of the 2012 NSTI Nanotechnology Conference and Expo,* NANOTech 2012 Volumes 1, 433-436.

Kotsilkova, R., & Tabakova, S. (2023). Exploring effects of graphene and carbon nanotubes on rheology and flow instability for designing printable polymer nanocomposites. *Nanomaterials,* 13(5), 835. https://doi.org/10.3390/nano13050835

Li, H., Li, Z., Qiu, L., Dong, S., Ouyang, J., Dong, X., & Han, B. (2023). Rheological behaviors and viscosity prediction model of cementitious composites with various carbon nanotubes. Construction and Building Materials, 379, 131214. https://doi.org/10.1016/j.conbuildmat.2023.131214

Liu, Y., Fu, C., Li, Y., Xu, W., Huang, Z., & Xu, Y. (2025). Uncovering hidden dangers in urban housing: Sources of indoor radon and associated health risks. Journal of Environmental Management, 387, 125899. https://doi.org/10.1016/j.jenvman.2025.125899

Mphaga, K. V., Mbonane, T. P., Utembe, W., & Rathebe, P. C. (2024). Short-Term vs. Long-Term: A Critical Review of Indoor Radon Measurement Techniques. *Sensors,* 24(14), 4575. https://doi.org/10.3390/s24144575

Park, S., & Kim, H. (2021). Enhanced barrier properties of polymer nanocomposite coatings using functionalized carbon nanotubes. *Journal of Applied Polymer Science, 138*(5), 49621. https://doi.org/10.1002/app.49621

Rashid, A. B., Haque, M., Islam, S. M., & Labib, K. R. U. (2024). Nanotechnology-enhanced fiber-reinforced polymer composites: Recent advancements on processing techniques and applications. *Heliyon,* 10(2), 1-29. https://doi.org/10.1016/j.heliyon.2024.e24692

Ruvira, B., García-Fayos, B., Juste, B., Arnal, J. M., & Verdú, G. (2022). Experimental estimation of the diffusion coefficient in radon barrier materials based on ISO/TS 11665-13: 2017. *Radiation Physics and Chemistry,* 193, 109993. https://doi.org/10.1016/j.radphyschem.2022.109993

U.S. Environmental Protection Agency (EPA). (2024). *A Citizen's Guide to Radon: The Guide to Protecting Yourself and Your Family from Radon.* EPA 402/K-23/002. https://www.epa.gov/sites/default/files/2016-12/documents/2016_a_citizens_guide_to_radon.pdf

Veselska, O., Vaidya, S., Llido, O., Macko, M., Deroche, I., Bourrelly, S., & Busto, J. (2025). Exploring the science of radon adsorption: Materials, methodologies, and emerging directions. Separation and Purification Technology, 134640. https://doi.org/10.1016/j.seppur.2025.134640

World Health Organization (WHO). (2023). *Radon and Health: Key Facts.* Retrieved from https://www.who.int/news-room/fact-sheets/detail/radon-and-health